MURAJ
Minnesota Undergraduate Research & Academic Journal
z.umn.edu/MURAJ

Automated quantitative analysis of silica nanorod dimensions via watershed segmentation

Michelle C. Quan, Christopher A. Neal, and Michelle A. Calabrese

Abstract

Quantifying the dimensions of silica nanorods often requires manual analysis of their dimensions, but this method is time consuming and tedious. This work explores the potential for an automated analysis with Matlab to improve the efficiency of this analysis. The program described is a preliminary proof-of-concept version of a nanorod analysis program. Watershed segmentation and bounding boxes are viable tools for the automated quantitative analysis of nanorod dimensions, and the automated process is far quicker than manual analysis. While the automated process shows promise, the program functions best with minimal nanorod overlap and requires more extensive testing to become feasible for widespread use. Improvements to noise reduction and particle shape prediction will expand the scope of images that can be subject to automatic analysis.

I. INTRODUCTION

Interest in smart materials and three-dimensional printing has grown in recent years, with innovation occurring in both fields. One area of research with overlap between these two categories regards four-dimensional (4D) printing. This printing consists of additive manufacturing of materials that can undergo a property change in response to external stimuli such as temperature changes or exposure to liquid [1]. One category of smart materials is those that change due to magnetic fields. Because magnetic fields are relatively nondestructive, properties can be changed without non-magnetic portions of the material incurring damage. Systems for 4D-printing of magneto-responsive materials commonly consist of a polymer embedded with magnetic materials like ferric oxide powders [2]. While these oxides can be oriented with magnetic fields, advancements could be continued with the introduction of nanoparticles into polymer matrices. Nanoparticle introduction can enable more precise variations in structure, allowing for more finely tuned composites and smart materials.

The program has a few key objectives. Nanorods must be distinguished from the background of the image. This requires image segmentation according to the difference in color of the background and the nanorods. The contrast level of the image can impact this difference. Next, the measurements for length and diameter must be taken. Given the relatively linear shape of most silica nanorods, the length taken by hand is along the mid-line of the nanorod, and the diameter is taken orthogonal to that bisector. The resulting dimensions must then be scaled from dimensions in pixels to the physical dimensions demonstrated by the scale bar.

When counting by hand, the scale is set before measuring dimensions, but matrix operations can be used after dimensions are taken to achieve this scaling in the program.

II. LITERATURE REVIEW

The majority of literature on the synthesis of silica nanorods utilizes similar synthesis procedures, despite differing reactant composition. The nanorods analyzed with this program were synthesized in a similar manner to Mitchell et al. [3] and Murphy et al. [6], [7]. Starting materials included polyvinylpyrrolidone (PVP), ethanol, Milli-Q water, aqueous sodium citrate dihydrate, ammonia, tetraethyl orthosilicate (TEOS), and either 1-pentanol or 1-octanol to dictate shape. After the reaction is initiated and left undisturbed overnight, the nanorods were sonicated, vortexed, and centrifuged to wash the products and remove leftover reactants. To prepare SEM samples, nanorod powders are suspended in ethanol and drop-cast onto a substrate. Scanning electron micrographs are then collected on a JEOL 6010 SEM. The resulting images are analyzed with ImageJ to measure diameter and length. While particle density may vary per image, between 30-60 particles are analyzed per sample [6].

Programs that quantitatively analyze area and segment images are not new, but application in anisotropic nanoparticle analysis is underutilized. Past work has been done with SEM images of spherical nanoparticles [8], measuring the single changing dimension, diameter, of particles. Given that nanorods have two independent dimensions, length and diameter, this procedure cannot be directly applied. However, image segmentation in other disciplines provides insight into methods that could work for this application. The edges of particles can e difficult to locate in M images due to the low threshold of difference in color that can occur etween the particles and the sample plate. ecause of this difficulty, watershed segmentation is a promising algorithm.

Topographically, a watershed is the raised area that separates two bodies of water of lower elevation, like rivers or drainage basins. This idea was expanded into image processing by sorting the pixels by their grey color [9]. This watershed algorithm is known for being accurate in finding the edges of particles even when the borders are weakly distinguishable [10]. Despite this accuracy, the algorithm also has some drawbacks. The algorithm is prone to over-segmentation of the image, finding borders where there are none. These can be remedied with the distance transformation, which relies on background pixels and pixels of interest. During a distance transformation, every pixel in the image is analyzed to find the nearest pixel of interest; in this procedure, the pixels of interest are the pixels that represent the nanorods. This helps to prevent over-segmentation because it preserves the existing borders [10]. The watershed algorithm for the nanorods is based on the order of operations outlined in Li et al. [11]. The original image is enhanced to remove noise and converted into a binary image. The binary image is then eroded to smooth the edges and filled in to avoid gaps before the watershed algorithm is applied. While Li's work focuses on the segmentation, the nanorod program has a quantitative component, so additional steps will be included to isolate the scale bar and measure the

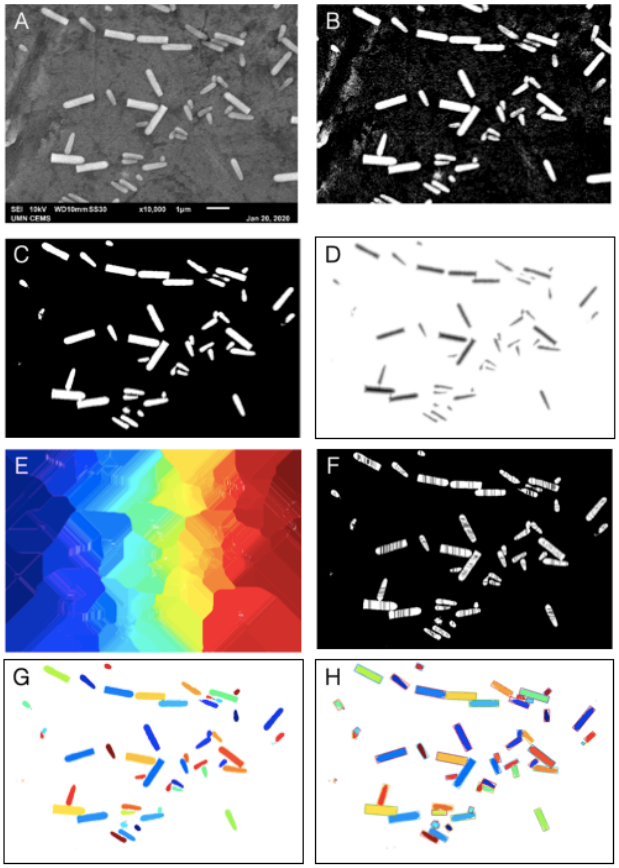

Figure 1. A series of images depicting key points in the image analysis process for Image I. Image A is the original image. Image B is the particles portion of the binary version of the image. Image C occurs after noise reduction, particle smoothing, and clearing of border particles. Image D is following the first distance transformation. Image E is the watershed transformation with RGB labels. Image F is the over-segmented image. Image G follows the second distance transformation with RGB labels. Image H is the final image with oriented boxes.

the particles.

III. RESEARCH METHODOLOGY

All SEM images to be analyzed are saved in the tagged image file format (.tif), and these images are selected manually to begin the program. Initial images are truecolor images stored in Matlab as RGB images with a three color channels [12] and converted to grayscale by identifying the dimension of the image. If the image has three dimensions, it is a truecolor image that must be converted to grayscale with the *rgb2gray* function in Matlab (all functions mentioned are standard Matlab functions unless otherwise specified). The resulting image still has extraneous text aside from the scale bar. So, the area is blacked out while avoiding the scale bar section. Thus, the image is split to separate the scale bar portion from the particles portion.

This split occurs along the edge of the information section to avoid cutting off particles. This turns the image without text into two images, the scale bar image and the particles image. On the scale bar image, the grayscale image is converted into a binary image with the imbinarize, and bwareaopen is used to eliminate any small regions of less than 100 pixels that may have been left out along the edges of the image [13]. Following this, imclearborder function is used to eliminate any regions touching the edges of the scale bar image to ensure the only region that is detected is the scale bar. The particles portion of the image undergoes a similar process to the example titled "Detect Cell Using Edge Detection and Morphology" from the Image Processing Toolbox User's Guide [12]. The image is converted into a binary image and particles smaller than 2000 pixels are eliminated to clear noise in the image. The majority of the nanorods are over 2000 pixels in size, so clearing clusters smaller than 2000 pixels is unlikely to clear any particles of interest. Then, the contrast is increased and the edges are dilated slightly to increase the clarity of the edges of particles. Then, holes within these confines are filled in and particles on the border of the image are eliminated.

Because the nanorods are often

touching each other, the particles image is subject to watershed segmentation based on a Matlab post by Steve Eddins [14]. To clear away background noise, bwareaopen is applied to the complement of the particles image and the complement of the resulting image is used. At this point, the particles of interest are white and the rest of the image is black. The majority of the noise is found in the background, but the function bwareaopen removes particles from the foreground, so this function is applied to the inverse of the image. The resulting image has a white background and black particles of interest, so the complement of the operation is taken at the end. A similar process is used for the distance transformation.

A distance transformation with bwdist measures the distance between every particle and the nearest particle of interest in white. Thus, the nanorods have zero distance to the nearest particle of interest because they are white and are marked as black catchment basins. While it is desirable to have the particles of interest be denoted as basins, this often fails to segment between touching particles of interest, so the process is less simple. The complement of the image displays the nanorods in black and the background in white as particles of interest. This results in the background of the image as well as the divisions between the particles being black pixels and the nanorods being white pixels. For the following watershed segmentation, the nanorods need to be labeled as basins, so the distance transformation is negated to make the nanorods basins [13].

After the watershed transformation, pixels in catchment basins have positive integers in the label matrix and watershed regions are labeled with zero. This is displayed with a function called *label2rgb* which demonstrates the colorful basins with the white watershed borders. To observe the impact on the nanorods, the watershed regions labeled in the matrix with zero are set to be black pixels and overlaid on the original binary particles image. This demonstrates the over-segmentation problem common in watershed segmentation [10]. To correct for this, the local minimums are filtered out to avoid the smallest minimums from becoming catchment basins and causing over-segmentation. A mask with the imextendedmin prevents local minima less than six from being denoted as basins [14]. The size of the local minima to be filtered out is determined by increasing the value and running the program until reaching a value that caused a loss of particles of interest. This mask is applied to the original distance transformation with the function imimposemin, eliminates the minima that led to the over-segmentation [12]. After this point, the aforementioned watershed process occurs again to finish the processing of the image.

The nanorod shape is most comparable to a rectangle or ellipse due to its anisotropy. The nanorod length and diameter are similar to a major and minor axis for these shapes, so Feret diameters are useful for this endeavor. The Feret diameter is the distance between two parallel planes tangent to the object. Given that the particle length and the diameter are typically orthogonal to each other, they can be used to create rectangular shapes that can enclose the nanorods. David Legland denotes these bounding rectangles with minimal area as "oriented boxes" [15]. His imOrientedBox function was used to measure the scale bar

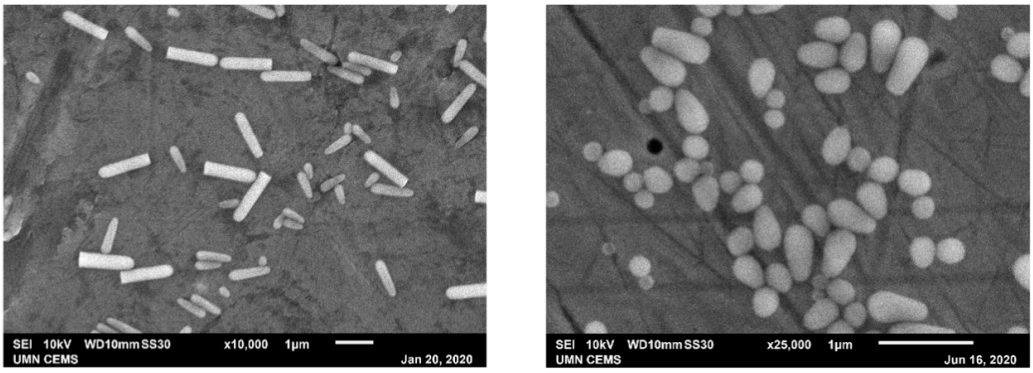

Figure 2. Original SEM images for two sets of particles. Image I (left) and Image II (right).

length as well as the nanorods. When applied to the scale bar portion of the image, the function returns a one by five matrix that displays the box center's x coordinate, y coordinate, length, width, and angle of rotation. At this point, the operator is prompted to enter the length of the scale bar in nanometers, and this, alongside the length of the scale bar in pixels allows for a pixels per unit scalar. When *imOrientedBox* is applied to the nanorods, the length and width columns are extracted and multiplied by the pixels per unit scalar to obtain the dimensions in nanometers. Despite previous noise removal and thresholding efforts, some of the edges of the particles are still identified separately. Thus, any identified boxes shorter than 50 nm in length or width are eliminated to reduce the impact of these discrepancies. From this new matrix, the average and standard deviation of the length and width of the nanorods are returned.

The automated process was tested on two different images. The images were selected for the lack of overlap between particles in order to test the accuracy of the program under more basic conditions. These images are denoted as Image I and Image II, both displayed in Figure 2. These images were also analysed manually using ImageJ. Three trials measuring length and diameter of the nanorods are averaged to create the manual data set that serves as the expected results for each of the images. Particles residing on the edges of the image are disregarded, but particles with slight overlap were recorded by estimating the edges of the nanorods that were not visible. For more irregular particles with varying diameters, as seen in Image II, the widest diameter is recorded.

IV. RESULTS

Due to the image segmentation and particle clearing process, the number of particles found by the automatic program and the number of particles counted by hand had some variation. A manual analysis of Image I consisted of 46 particles whereas the automatic analysis found 52 particles. Table I depicts the average dimensions for both methods and dimensions for length and width for the entire population recorded by both methods are displayed in Figure 3.

The manual and automatic results are compared with an unpaired t-test to determine if the deviation in results is statistically significant. The equations used for these calculations can be found in Appendix A. For

Table I. Average and standard deviation of manual and automatically obtained nanorod length and diameter for Image I

Parameter	Method	Average ± SD (nm)
Length	Manual	380 ± 130
	Automatic	330 ± 130
Diameter	Manual	270 ± 38
	Automatic	240 ± 45

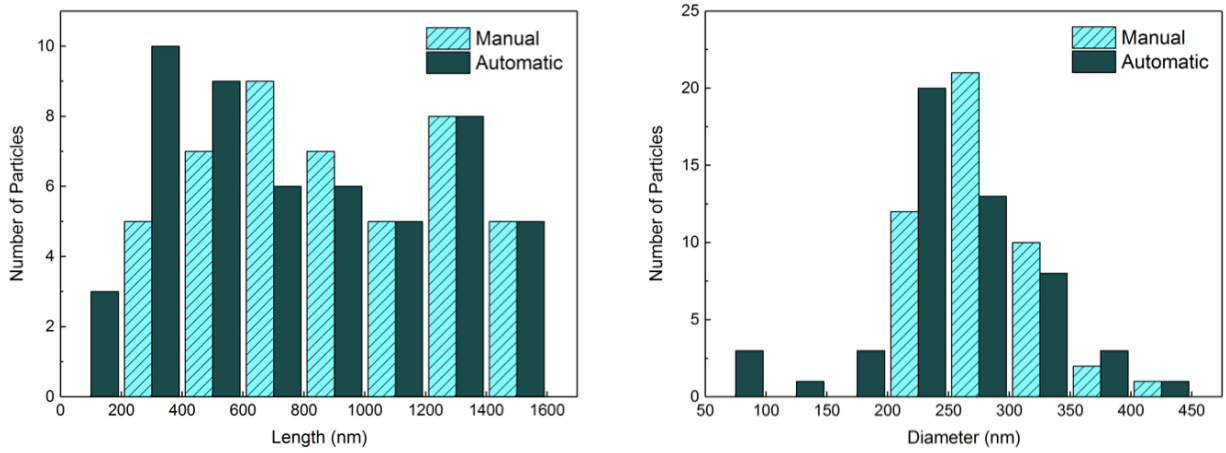

Figure 3. Image I nanorod length (left) and diameter (right) via manual and automatic methods.

length, and equal variance t-test is conducted because Fcalc < Ftable, and, for width, an unequal variance t-test is conducted because Fcalc > Ftable. In either case, if tcalc < ttable, there is no statistically significant difference between the average values obtained automatically versus manually at the 95% confidence level. These values are displayed in Table II.

In cases where the degrees of freedom are between two values on the reference table, the lower degree of freedom was used to maintain a conservative estimate. There is no statistically significant difference in average length obtained automatically versus manually at the 95% confidence level, but the average diameter obtained automatically has a statistically significant difference than the average found manually.

For Image II, a manual analysis identified and measured 48 particles whereas a manual analysis found 49 particles. The average and standard deviation of the nanorods dimensions are displayed for each method in Table III with histograms for the entire population in Figure 4.

Once again, an unpaired t-test is used to compare the averages from the manual and automatically obtained data to determine if differences are statistically significant. In Image II, both length and width were determined to have equal variance between the manual and automatic data via the F-test. Thus, an equal variance t-test was used for both length and diameter. Calculated and reference F and t values can be found in Table IV.

For Image II at the 95% confidence level, the automatically obtained average nanorod length is not statistically significantly different from the average nanorod length measured

Table II. Relevant calculated and reference statistical values for average length and diameter of nanorods in Image I

Parameter	Statistic	Calculated Value	Reference Table Value ($\alpha = 0.05$)
Length	F	1.33	1.6928
	t	1.52	1.990
Diameter	F	2.43	1.6928
	t	1.99	1.990

Table III. Average and standard deviation of manual and automatically obtained nanorod length and diameter for Image II

Parameter	Method	Average $\pm$ SD (nm)
Length	Manual	380 ± 130
	Automatic	330 ± 130
Diameter	Manual	270 ± 38
	Automatic	240 ± 45

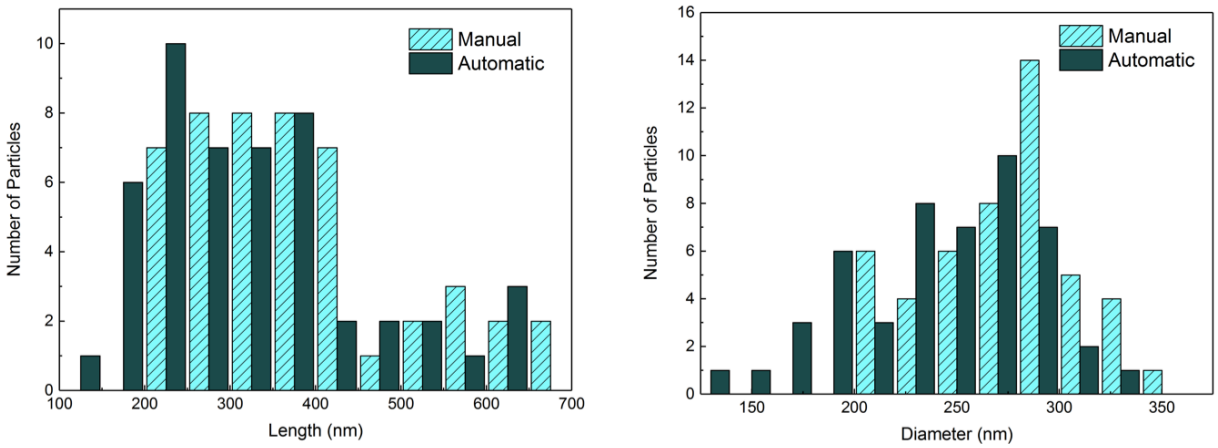

Figure 4. Image II nanorod length (left) and diameter (right) via manual and automatic methods.

manually. However, at this confidence level, the average nanorod diameter from the automatic and from the manual data sets demonstrate a statistically significant difference.

In both Image I and Image II, the automatic averages for both length and width were lower than the manually obtained averages. This is demonstrated by Figure 5.

V. DISCUSSION

Scratches may explain the tendency of automated measurements being smaller than the manual measurements on the plate. In both cases, the automated process observed more particles than the manual process. These particles may be attributed to plate scratches or other surface irregularities that are detected by the program. These irregularities tend to be smaller than the particles themselves due to the noise reduction efforts that occurs in image processes. However, to avoid excluding small particles, the final threshold eliminates boxes smaller than 50 nm by 50 nm, so scratches that are above this length or width are still included in the final averages. Use of more pristine sample plates as well as improvements in the image segmentation process would both reduce this issue. Because the automated data set included more particles than the manual data set, a paired t-test could not be performed with

Table IV. Relevant calculated and reference statistical values for average length and diameter of nanorods in Image II

Parameter	Statistic	Calculated Value	Reference Table Value ($\alpha = 0.05$)
Length	F	1.01	1.6928
	t	1.81	1.990
Diameter	F	1.38	1.6928
	t	3.80	1.990

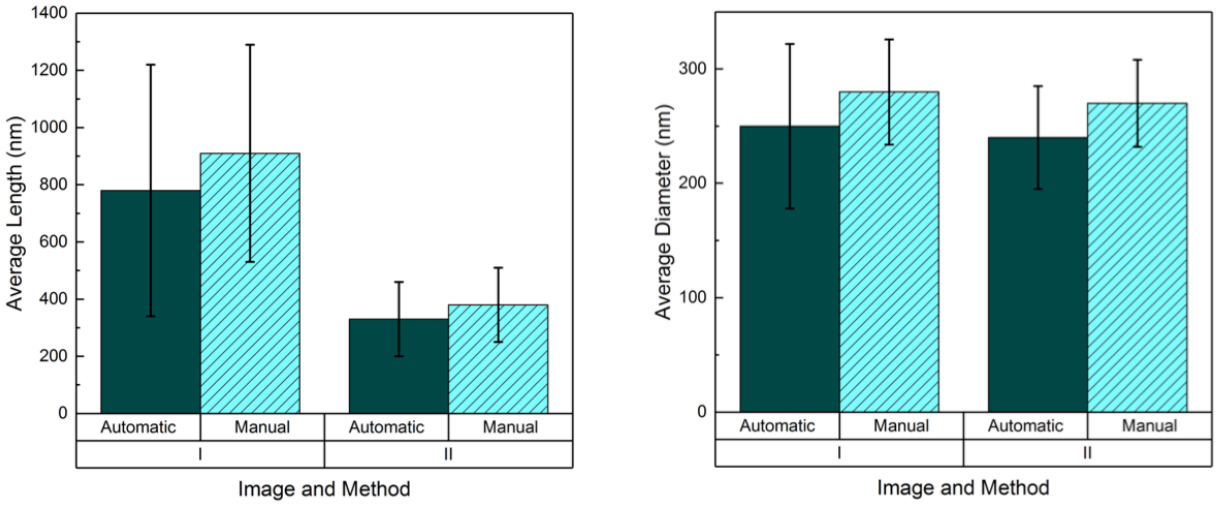

Figure 5. Average and standard deviation (denoted by error bars) of dimensions from particles in Image I and II obtained by manual and automatic means.

the raw data. Given that the same images were analyzed with both methods, a paired t-test would have been more appropriate for this analysis. Thus, the use of an unpaired t-test may have contributed to the differences observed.

This difference in averages could also be caused by the irregular particles contained in both images. Proper nanorod growth would have a flat end and a domed end, forming a half discorectangle shape similar to a test tube. However, these images contain an amalgamation of these nanorods as well as irregular nanoparticles with a rounded teardrop shape that lacks a flat edge. Because of this, the irregular particles can be enclosed by an oriented box at an angle, shown in Figure 6.

When the flat side of the nanorod is tangent to the bounding box, the width of the bounding box corresponds to the diameter of the nanorod and the length of the bounding box equals the length of the nanorod. In the irregular cases, the length of the nanoparticle becomes a hypotenuse of a right triangle whose legs are parallel to the length and width of the oriented box. Because of this, the oriented box length and width generated as smaller than the actual length and diameter of the nanoparticle. The particles in both of these images were synthesized with different starting materials or reactant ratios, causing more irregularity in shape. Thus, the decrease caused by this shape could be reduced in samples with synthesis processes that align more closely with previous literature.

A key flaw in the current iteration of the program is the difficulty discerning overlapping

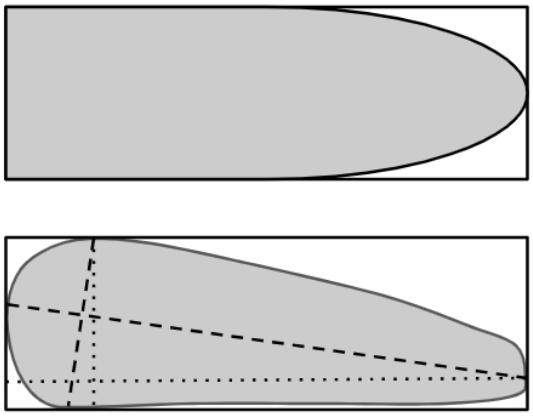

Figure 6. A comparison of imOrientedBox on a test tube shape (top) and rounded raindrop shape (bottom). Dashed lines indicate how the particle's length and width would be analyzed manually and dotted lines are parallel to the sides of the box.

or closely packed particles. The images used to test the analysis were chosen because they had dispersed particles with minimal overlap. However, many images of the particles are not this well dispersed, and the program struggles to segment the image properly in these cases. With overlap, more shadows are visible on the nanorods, so converting the image from true color to binary causes many particles to be missed or fragmented. When the particles are densely packed, particles may also be deleted in the border clearing process. While imclearborder is intended to clear just the particles touching the border, particles that are touching the particles on the border can also be removed because they are believed to be connected. With more closely packed samples, a larger percentage of the nanorod population is touching nanorods that are cut off by the border of the image. This results in fewer nanorods reaching the watershed process. These problems are demonstrated in Figure 7.

The majority of images of the nanorods have clumps or sheets of nanorods due to the drop-casting technique used to deposit the samples onto the plates. Diluting the sample with more solvent would improve separation of nanorods by reducing the density of nanorods in the drop that is deposited onto the sample plate. Using a more volatile solvent could also reduce clumping. The nanorods within the droplet have more time to clump together if the solvent takes longer to evaporate. Therefore, a more volatile solvent with a reduced evaporation time may result in fewer clusters of nanorods.

Aside from improvements to the drop-casting process, improvements could be made to the program itself. Overlap of objects that need to be analyzed is not unique to nanoparticles, and some of the processes that have been used in other fields may be applicable. A combination of seed detection with level set active contour has been used to segment overlapping cells [16]. In the case of cells, the number of cells in the image was estimated based on the nuclei as seed points. While the nanorod shapes are less circular than cells and lack nuclei, the particles curved shape have high points that are lighter than the rest of the particle. If these lighter points could be identified as seed points in a similar fashion, an estimation of the nanorod population in the image could be made and this could be followed by level set active contour to segment the particles even when overlap occurs. The idea of segmenting based on contour is not new, and it has been discussed as a way to segment images that have occluded objects. Concave point detection coupled with polygonal approximation has been proposed as a solution to segmentation problems that are caused by

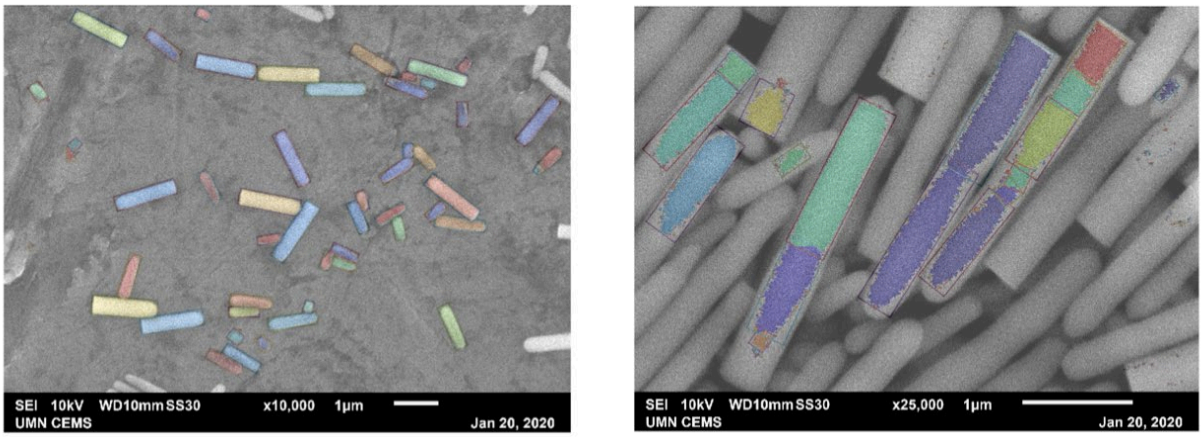

Figure 7. A comparison of Image I (left) versus a more densely packed image (right). The final images with oriented boxes are overlaid on the original SEM images to compare which nanorods are identified.

overlapping convex shapes [17]. Although the proposed method was tested on transmission electron microscopy images of elliptical nanoparticles, polygonal approximation could be applied to nanorods as well.

VI. CONCLUSION

This program is a promising exploration into automating the quantitative analysis of nanorods. For the images tested, the results for nanorod length from the automated process had a statistically insignificant difference to the results from the manual process. Although the difference in average nanorod diameter between the two methods was statistically significant, these differences can be mitigated by improving the drop-casting technique. The program itself requires more extensive testing and alterations to allow a larger variety of images to be analyzed properly, but the current iteration serves as a proof-of-concept. Even in its current form, it can aid in the advancement of research regarding the synthetic control of silica nanorods. This dimensional data will be useful for potential future work intended to explore the impact of doping the nanorods with iron or creating hollow nanorods. With optimal dispersion of nanorods across the plate, it can quickly provide estimates on the dimensions of the nanorods and make analysis more efficient.

ACKNOWLEDGEMENT

This research was primarily funded by the Multicultural Summer Research Opportunities Program (MSROP) through the Office of Undergraduate Research (OUR) at the University of Minnesota, Twin Cities. I would like to thank Vicky Munro (OUR Associate Director) and Heidi Fahning (OUR Program Coordinator) for the opportunity to participate in MSROP.

I also extend my gratitude to my mentors, Dr. Michelle A. Calabrese (Assistant Professor in the Department of Chemical Engineering and Materials Science) and Christopher A. Neal (graduate student in the Department of Chemical Engineering and Materials Science) for their guidance and support throughout this process.

APPENDIX A
Equations for statistical analysis

These equations use averages ($\bar{x}_i$) standard deviations (SD_i) and population size (n_i).

$$F_{calc} = \frac{(SD_1)^2}{(SD_2)^2}, \qquad SD_1 > SD_2 \tag{A.1}$$

An equal variance t-test occurs if $F_{calc} < F_{table}$.

$$s_{pooled} = \sqrt{\frac{(SD_1)^2(n_1 - 1) + (SD_2)^2(n_2 - 1)}{n_1 + n_2 - 2}} \tag{A.2}$$

$$t_{calc} = \frac{|\bar{x}_1 - \bar{x}_2|}{s_{pooled}} \sqrt{\frac{n_1 n_2}{n_1 + n_2}} \tag{A.3}$$

$$Df = n_1 + n_2 - 2 \tag{A.4}$$

An unequal variance t-test occurs if $F_{calc} > F_{table}$.

$$t_{calc} = \frac{|\bar{x}_1 - \bar{x}_2|}{\sqrt{\frac{(SD_1)^2}{n_1} + \frac{(SD_2)^2}{n_2}}} \tag{A.5}$$

$$Df = \frac{\left(\frac{(SD_1)^2}{n_1} + \frac{(SD_2)^2}{n_2}\right)^2}{\frac{\left(\frac{(SD_1)^2}{n_1}\right)^2}{n_1 - 1} + \frac{\left(\frac{(SD_2)^2}{n_2}\right)^2}{n_2 - 1}} \tag{A.6}$$

REFERENCES

[1] Z. X. Khoo, J. E. M. Teoh, Y. Liu, C. K. Chua, S. Yang, J. An, K. F. Leong, and W. Y. Yeong, "3d printing of smart materials: A review on recent progresses in 4d printing," Virtual and Physical Prototyping, vol. 10, no. 3, pp. 103–122, 2015.

[2] Z. Zhang, K. G. Demir, and G. X. Gu, "Developments in 4d-printing: a review on current smart materials, technologies, and applications," International Journal of Smart and Nano Materials, vol. 10, no. 3, pp. 205–224, 2019.

[3] K. K. Pohaku Mitchell, A. Liberman, A. C. Kummel, and W. C. Trogler, "Iron (iii) doped, silica nanoshells: a biodegradable form of silica," Journal of the American Chemical Society, vol. 134, no. 34, pp. 13997–14003, 2012.

[4] A. Spaggiari, D. Castagnetti, N. Golinelli, E. Dragoni, and G. Scirè Mammano, "Smart materials: Properties, design and mechatronic applications," Proceedings of the Institution of Mechanical Engineers, Part L: Journal of Materials: Design and Applications, vol. 233, no. 4, pp. 734–762, 2019.

[5] I. I. Slowing, B. G. Trewyn, S. Giri, and V.-Y. Lin, "Mesoporous silica nanoparticles for drug delivery and biosensing applications," Advanced Functional Materials, vol. 17, no. 8, pp. 1225–1236, 2007.

[6] R. P. Murphy, K. Hong, and N. J. Wagner, "Synthetic control of the size, shape, and polydispersity of anisotropic silica colloids," Journal of colloid and interface science, vol. 501, pp. 45–53, 2017.

[7] R. P. Murphy, K. Hong, and N. J. Wagner, "Thermoreversible gels composed of colloidal silica rods with short-range attractions," Langmuir, vol. 32, no. 33, pp. 8424–8435, 2016.

[8] L. Crouzier, A. Delvallée, S. Ducourtieux, L. Devoille, C. Tromas, and N. Feltin, "A new method for measuring nanoparticle diameter from a set of SEM images using a remarkable point," Ultramicroscopy, vol. 207, p. 112847, 2019.

[9] L. Vincent and P. Soille, "Watersheds in digital spaces: an efficient algorithm based on immersion simulations," IEEE Transactions on Pattern Analysis & Machine Intelligence, no. 6, pp. 583–598, 1991.

[10] Y. Zhao, J. Liu, H. Li, and G. Li, "Improved watershed algorithm for dowels image segmentation," in 2008 7th World Congress on Intelligent Control and Automation, pp. 7644–7648, IEEE, 2008.

[11] H. Li, G. Sun, H. Sun, and W. Liu, "Watershed algorithm based on morphology for dental x-ray images segmentation," in 2012 IEEE 11th International Conference on Signal Processing, vol. 2, pp. 877–880, IEEE, 2012.

[12] Mathworks, Natick, MA, Image Processing Toolbox User's Guide, 2020. Release 2020a.

[13] Mathworks, Natick, MA, Image Processing Toolbox Reference, 2020. Release 2020a.

[14] S. Eddins, "Watershed transformation question from tech support." Available at https://blogs.mathworks.com/steve/2013/11/19/watershed-transform-question-from-tech-support/ (2013/11/19). Retrieved July 18, 2020.

[15] D. Legland, "Feret diameter and oriented box." MATLAB Central File Exchange. Available at https://www.mathworks.com/matlabcentral/fileexchange/30402-feret-diameter-and-oriented-box (2014/09/02). Retrieved July 20, 2020.

[16] X. Qi, F. Xing, D. J. Foran, and L. Yang, "Robust segmentation of overlapping cells in histopathology specimens using parallel seed detection and repulsive level set," IEEE Transactions on Biomedical Engineering, vol. 59, no. 3, pp. 754–765, 2011.

[17] S. Zafari, T. Eerola, J. Sampo, H. Kälviäinen, and H. Haario, "Comparison of concave point detection methods for overlapping convex objects segmentation," in Scandinavian Conference on Image Analysis, pp. 245–256, Springer, 2017.